PCCP

Accepted Manuscript

ROYAL SOCIETY OF CHEMISTRY

www.rsc.org/pccp

Influence of hybrid nano-filler on the crystallization behaviour and interfacial interaction in polyamide 6 based hybrid nano-composites

M. S. Sreekanth[a], Ajay S. Panwar[a], Petra Pötschke[b], Arup R. Bhattacharyya[a*]

[a]Department of Metallurgical Engineering and Materials Science, Indian Institute of Technology Bombay, Powai, Mumbai 400076, India

[b]Department of Functional Nanocomposites and Blends, Leibniz Institute of Polymer Research Dresden, HoheStrasse 6, D-01069 Dresden, Germany

Abstract

Expanded graphite (EG) and multiwalled carbon nanotubes (MWNTs) based hybrid nano-composites were prepared with polyamide 6 (PA6) matrix via melt-mixing technique using a conical twin-screw micro-compounder. A novel organic modifier (lithium salt of 6-aminohexanoic acid; Li-AHA) was employed to modify MWNTs, which was utilized to intercalate Li-AHA modified MWNTs into the partially exfoliated EG gallery. Morphological investigation showed the intercalation of Li-AHA modified MWNTs into partially exfoliated EG gallery in EG/MWNTs-m2h hybrid, whereas unmodified EG/MWNTs-h hybrid mixture exhibited a separate identity in the mixture. Improved interaction via melt-interfacial reaction between acid end group of PA6 and amine functionality of Li-AHA in EG/MWNTs-m2h hybrid filler was confirmed by Fourier transform infrared spectroscopic analysis. The extent of melt-interfacial reaction was increased as a function of Li-AHA concentration in the filler. Wide angle X-ray diffraction analysis showed the existence of α-crystalline phase of PA6. The incorporation of MWNTs, EG and EG/MWNTs hybrid in the PA6 matrix has favoured α-crystalline structure of the PA6 phase. Crystallization studies have indicated a significant increase in bulk crystallization temperature of the PA6 phase in the presence of MWNTs, EG and EG/MWNTs hybrid filler. Moreover, the formation of PA6 ‘trans-crystalline lamellae’ on MWNTs surface

was facilitated in case of composites with MWNTs and EG/MWNTs hybrid filler. An attempt has been made to investigate the role of EG/MWNTs hybrid filler in influencing the crystallization behaviour of the PA6 phase in the hybrid nano-composites.

Keywords: expanded graphite, multiwalled carbon nanotubes, polyamide 6, crystallization, hybrid nanocomposites

* Author to whom all the correspondence should be addressed:

E-mail: arupranjan@iitb.ac.in, Tel. No.: +91-22-2576-7634, Fax: +91-22-2572-6975

Introduction

Carbon nano-fillers incorporated polymer nano-composites exhibit extraordinary mechanical, thermal, electrical and barrier properties [1-3], which could be utilized to develop high strength materials for structural applications, energy storage devises, EMI shielding and sensor applications [4, 5]. The properties of the polymer nano-composites depend primarily on the dispersion state of the filler and the interfacial interaction between the filler and the polymer matrix. Graphene and carbon nanotubes (CNTs) have been considered as the most important candidates under the 'nano-materials' category, which exhibit outstanding tensile strength and tensile modulus, with unique electrical and thermal conductivity and of very high surface/volume ratio [1, 2].

The concept of hybrid filler has been introduced in recent time to make use of the unique properties associated with the individual filler constituting the hybrid. Hybrids fillers could be developed by the combination of different carbon based nano-fillers with varying dimensionality, which may lead to a synergistic effect on various properties of polymer matrices [6-8]. The main challenge associated with graphene lies with the 'restacking' phenomenon, whereas, CNTs exhibit 'agglomeration' behaviour in the as-received sample and also in the corresponding polymer nano-composites. The utilization of the hybrid filler via the combination of graphene and CNTs could resolve the issue of 'restacking' and 'agglomeration' up to certain extent [9, 10]. A significant improvement in mechanical, electrical and thermal properties of CNTs and graphene based hybrid nano-composites over individual fillers has been demonstrated earlier. An exemplary improvement in gravimetric toughness of 1000 J/g was achieved in polyvinyl alcohol (PVA) composite fibre via the use of 1:1 (wt/wt) hybrid mixture of reduced graphene oxide (RGO) and single walled carbon nanotubes (SWNTs), which was significantly higher than the

individual filler based composite fibre [6]. An enhanced thermal conductivity up to 800% was observed in epoxy composites consisting of 3:1 (wt/wt) hybrid of graphite nano-platelets (GNP) and SWNTs, which was much higher than the corresponding composite of either GNP (600%) or SWNTs (300%) [7]. A synergistic effect in DC electrical conductivity of ~41 S/cm was observed for poly (lactic acid) (PLA) composite at 12 vol.% concentration of the hybrid filler consisting of 1:3 (wt/wt) hybrid of CNTs and expanded graphite (EG) [8].

The role of interfacial interaction between the nano-filler and the polymer matrix is a crucial factor in developing polymer nano-composites with enhanced properties. In this context, the crystallization behaviour of the semi-crystalline polymer influences significantly the mechanical properties of the corresponding nano-composites. The hetero-nucleating effect of MWNTs and EG in various semi-crystalline polymer matrices has been documented earlier [11-14]. The crystallization behaviour of polyamide 6 (PA6) in PA6/MWNTs composites showed the existence of 'trans-crystalline lamellae' of PA6 on the surface of MWNTs, which depict double crystallization exothermic peak at temperature higher than the bulk crystallization temperature (T_c) of PA6 [11, 15]. Semi-crystalline morphology of PA6/CNTs composites was investigated via wide angle X-ray diffraction analysis [11, 12]. PA6 crystallizes either in α and/or γ-crystalline forms [16]. Among these, α-crystalline form is thermodynamically more stable than γ-crystalline form, which is influenced by several factors viz., processing protocol and cooling strategy during injection moulding [14, 17]. Rapid cooling and lower crystallization temperature promotes the α-crystalline structure of PA6, whereas higher crystallization temperature or slow cooling leads to γ-crystalline structure [17]. Further, the hybrid mixture of CNTs and graphene may act as a hetero-nucleating agent, which may reduce the solidification time during processing and control the crystal size and crystal size distribution of the PA6 phase. In case of fiber

processing, the anisotropic structure related to hybrid mixture may significantly influence the crystalline morphology associated with the polymer matrix.

It has been observed that incorporation of CNTs in PA6 significantly improves the mechanical properties, electrical conductivity and thermal properties [12, 18] of PA6/CNTs composites. However, the extent of 'agglomeration' of MWNTs in PA6 matrix could be reduced significantly by the use of a non-covalent organic modifier [19]. In view of this, it has been planned to investigate the influence of pristine as well as organically modified MWNTs based hybrid filler of EG/MWNTs on the crystallization behaviour of the PA6 matrix. Moreover, it is envisaged that organically modified MWNTs may intercalate in the partially exfoliated EG gallery of the hybrid mixture of EG/MWNTs. In this context, the crystallization behaviour of the PA6 phase in the corresponding hybrid nano-composite may as well highlight the interfacial interaction between PA6 and the hybrid filler.

Experimental

Materials

Polyamide 6 (PA6, with zero shear viscosity of 180 Pa.s at 260 °C) was obtained from GSFC, Gujarat, India (Gujlon M28RC, relative viscosity 2.8, M_v is 38642 in 85% formic acid). Multiwalled carbon nanotubes (MWNTs) synthesized by CCVD method were obtained from Nanocyl SA, Belgium (NC-3100, average length: 1.5μm, average diameter: 9.5nm, purity: 95% as per manufacturer specification). Expanded graphite (EG) was supplied by Asbury carbon, USA (3806, average particle size of < 20μm and specific surface area of ~23.4 m^2/g as per manufacturer specification). 6-aminohexanoic acid (AHA) (Merck, Germany, M_w = 131.17; purity: 99%) was neutralized using lithium hydroxide (S. D. Fine-Chem Limited, India, purity: 99%) to obtain lithium salt of 6-aminohexanoic acid (Li-AHA).

Modification of filler

Pristine MWNTs were modified with Li-AHA in the ratio of 1:1 (wt/wt) and 1:4 (wt/wt) (MWNTs:Li-AHA) as reported earlier [20]. MWNTs were initially dispersed in de-ionized water by ultra-sonication (Bath ultra-sonicator, Vibronics, India, frequency 20 KHz) for 10 min. Required amount of Li-AHA was dissolved in deionized water and was then slowly added to aqueous dispersion of MWNTs and further sonicated for 20 min. The resultant dispersion was continuously heated and stirred over a hot plate at 100 °C to obtain dry mixture of Li-AHA modified MWNTs. It was then dried in a vacuum oven at 80 °C for 24 h to remove the traces of water. Li-AHA modified EG was also prepared in a similar manner described above. Hereafter, 1:1 (wt/wt) and (1:4) (wt/wt) Li-AHA modified MWNTs are denoted as m1-MWNTs and m2-MWNTs respectively. Similarly, 1:1 (wt/wt) Li-AHA modified EG is denoted as m-EG. Subsequently, a mixture of hybrid filler consisting of pristine MWNTs and pristine EG in the ratio of 1:4 (wt/wt) EG:MWNTs was prepared by ultra-sonication in tetrahydrofuran (THF) for 20 min and the solvent was evaporated at room temperature. The hybrid mixture was kept in the vacuum oven for 24 h to remove the traces of solvent. Further, a mixture of hybrid filler consisting of EG and Li-AHA modified MWNTs [EG:MWNTs of 1:4 (wt/wt)] was prepared by ultra-sonication of EG and m1-MWNTs in deionized water for 45 min (optimized by UV-visible spectroscopic investigation). The resultant dispersion was dried as described earlier. Hereafter, hybrid mixture consisting of pristine EG and pristine MWNTs is denoted as EG/MWNTs-h, whereas hybrid mixtures consisting of EG and m1-MWNTs/m2-MWNTs are denoted as EG/MWNTs-m1h and EG/MWNTs-m2h.

Sample Preparation

PA6, MWNTs, EG and EG/MWNTs-h, EG/MWNTs-m1h, EG/MWNTs-m2h hybrid mixtures were vacuum dried at 80 °C for 12 h prior to melt-mixing. Composites of PA6 with MWNTs, EG and EG/MWNTs-h were prepared by melt-mixing in a conical twin-screw micro-compounder (Micro 5, DSM Research, Netherlands) at 260 °C with a rotational speed of 150 rpm for 10 min. Melt-mixing was performed under nitrogen atmosphere in order to prevent any oxidative degradation. The concentration of the filler in the PA6 matrix was varied from 1-5 wt%. Composite film of ~0.2 mm was prepared by compression moulding at 260 °C.

Characterizations

Morphological investigations of MWNTs, EG and EG/MWNTs-h hybrid mixtures were investigated via scanning electron microscopic (FEG-SEM, JSM-7600F, JEOL, Japan) analysis and transmission electron microscopic (FEG-TEM, JEM-2100F, JEOL, Japan) analysis. The crystalline morphology associated with graphitic structure was determined using selected area electron diffraction (SAED) analysis during TEM investigation. Extrudates of the respective composites were cryofractured in the liquid nitrogen. The cryofractured surface of the composite was gold sputtered to avoid charging of the sample. The morphology of the composite was observed using SEM (S3400N, Hitachi, Japan). Ultra-thin section of ~60-70 nm was prepared using Leica Ultra-microtome Micro-systems (Germany) for TEM investigation. Further, samples were collected on a TEM grid and the investigation was carried out with a FEG-TEM (JEM-2100F, JEOL, Japan) equipment.

BET specific surface area measurements were carried out for pristine MWNTs, EG and EG/MWNTs-h hybrid mixtures using BET surface area analyzer (Smart Instruments, India), which is working on the principle of nitrogen adsorption.

Raman spectroscopic analysis was used to investigate the ordered and disordered state of carbon in MWNTs, EG and various hybrid fillers of EG/MWNTs mixture. Raman spectroscopic analysis was performed using a HR 800 micro Raman (HORIBA, Jobin Yovon, France) on powder samples in the scanning range of 1000 to 3000 cm^{-1}. The laser light wavelength of 514 nm was used with 10 mW power.

Wide angle X-ray diffraction (WAXD) analysis was carried out with a PANalytical X-Ray diffractometer (Philips, The Netherlands). The incident X-rays (λ=1.54 Å) from the Cu-target were monochromatized using a Ni filter. WAXD patterns were recorded with a step scan with step size of 0.02 between 5° and 40° (2θ). WAXD analysis was carried out for EG, MWNTs, EG/MWNTs hybrid filler and the corresponding composites of PA6. Crystallite size of PA6 was calculated using Scherrer's formula as shown by equation (1) in the respective composites.

$$D = \frac{0.9\lambda}{\beta cos\theta} \quad (1)$$

where, D is the crystallite size, λ is the wavelength of the incident X-Ray, β is the full width at half maxima (FWHM) in radian, $\beta = \beta' - \beta_0$ where β' is the observed FWHM and β_0 is the FWHM due to instrumental broadening.

Fourier transform infra-red spectroscopic (FTIR) analysis was carried out using a MAGNA 550 FTIR spectrometer (Nicolet, USA) for powder samples of PA6 composites with m2-MWNTs and EG/MWNTs-m2h. The composite samples were analyzed over the scanning range of 400-4000 cm^{-1} at room temperature. KBr pellet was used for calibration purpose.

Differential scanning calorimetric (DSC) analysis was performed with a modulated DSC (Q200, TA instruments, USA) under nitrogen atmosphere. Extrudate samples of about 5-6 mg

were dried in a vacuum oven at 80 °C for 12 h prior to the experiment. The samples were initially heated to 260 °C and kept for 3 min to delete any previous thermal history. Samples were then cooled to -40 °C at a cooling rate of 10 °C/min and the crystallization exotherms were recorded. After the samples were cooled to -40 °C at 10 °C/min, again heated to 260 °C at the heating rate of 10 °C/min, where the melting endotherm for the samples were recorded. The degree of crystallinity (X_c) of PA6 phase in the multi-component system was calculated using equation (2).

$$X_c = \frac{\Delta H_m}{\Delta H^\circ_m \times \phi} \times 100 \quad (2)$$

where, ΔH_m is the normalized heat of fusion corresponding to the PA6 phase in the blends, ΔH_m^o is the heat of fusion of 100% crystalline PA6 phase and ϕ is the weight fraction of the PA6 phase present in the composite. The heat of fusion of 100% crystalline PA6 was considered as 204.8 J/g [20].

Results and Discussion

a. Morphology of pristine MWNTs, pristine EG and hybrid mixture of EG/MWNTs

The morphology of carbon based fillers such as pristine and Li-AHA modified MWNTs, EG and hybrid fillers of EG/MWNTs were investigated using FEG-SEM and FEG-TEM observations as shown in Fig. 1. MWNTs exhibit cylindrical structure consisting of concentric walls, which exist as 'agglomerates' [21]. TEM analysis shows the existence of entangled MWNTs network; MWNTs consist of 6-8 concentric cylinders with average diameter of D_{avg}=~ 9±3 nm. SEM observation also indicates an 'entangled' MWNTs network having porous structure. Ultra-sonication of pristine MWNTs was not sufficient enough for effective 'debundling' of the MWNTs 'agglomerates'. It is clearly seen from the TEM micrograph (Fig. 1)

that 'debundling' of MWNTs is observed upon modification with non-covalent modifier; Li-AHA [19]. The modification of MWNTs via Li-AHA leads to an increase in D_{avg} (~ 10.5±2 nm) due to the adsorbed Li-AHA on the surface of MWNTs. Further, the corresponding SEM micrographs of pristine and Li-AHA modified MWNTs show an 'entangled' network of MWNTs. The 'agglomerates' strength of MWNTs may decrease with Li-AHA modification due to effective 'debundling'.

It is to be noted that 'agglomeration' of MWNTs is due to inter-tube van der Waals force of attraction. In order to overcome the 'agglomeration' of MWNTs, non-covalent modification of MWNTs with Li-AHA has been employed to improve the dispersion extent of MWNTs. The mechanism of 'debundling' of MWNTs by using Li-AHA like modifier has been earlier proposed via electrostatic charge repulsion between AHA^- and the negative charges of MWNTs in the aqueous dispersion [22, 23]. Improved dispersion of MWNTs was achieved earlier by using sodium salt of 6-aminohexanoic acid (Na-AHA) in the PA6 matrix [19]. The extent of 'debundling' of MWNTs has significantly increased at higher concentration of Na-AHA. BET analysis suggests the adsorption of Li-AHA on MWNTs surface in the solid powder sample as the specific surface area (Table 1) corresponding to pristine MWNTs decreases significantly with Li-AHA modification.

Raman spectrum of pristine MWNTs shows the G band at ~1577 cm^{-1} and D band at ~1343 cm^{-1}corresponding to bond stretching vibrations of sp^2 domains of graphitic structure and disordered induced peak respectively [24] in Fig. 1. Raman spectrum of m1-MWNTs shows an up-shift in G band to 1583 cm^{-1} [23] due to 'debundling' of MWNTs in the presence of Li-AHA. Pristine MWNTs show I_D/I_G ratio of 1.1 due to the presence of defects, whereas m1-MWNTs show I_D/I_G ratio of 0.9 due to improved 'debundling'. Raman spectrum of m1-MWNTs (Fig. 1)

shows a shift in G-band to higher wave number as compared to pristine MWNTs, which may originate from 'CH-π' type of interaction [25]. The shift in G-band may also attribute to the 'debundling' of MWNTs in the presence of Li-AHA. Further, the electrostatic charge repulsion between MWNTs in the presence of Li-AHA may also contribute to a hydrostatic pressure on MWNTs surface. I_D/I_G ratio of m1-MWNTs shows a lower value as compared to pristine MWNTs due to the presence of more exposed sp^2 domains due to 'debundling' of MWNTs [23]. Morphological investigation of EG shows (Fig. 1) 'platelet-like' structure with varying layer thickness and of varying size corresponding to the respective platelet. EG exhibits multi 'pore-like' structure due to expansion [26], which may enable to establish better interaction with the polymer matrix [21]. EG exhibits very high thickness as shown in Fig. 1. Selected area electron diffraction (SAED) analysis of EG depicts 'ring-like' pattern corresponding to 'polycrystalline' nature of EG. Non-covalent modification of EG with Li-AHA leads to further exfoliation of EG to few layer 'graphene-like' structure, which is exhibited by 'hexagonal' dot pattern in the SAED analysis [27].

EG exists as 'stacked' platelets due to van der Waals forces of attraction between the layers. TEM micrograph of m-EG shows the 'exfoliation' or 'de-stacking' of EG due to electrostatic repulsion, which is also observed in the case of m-MWNTs. Further, the decrease in specific surface area from BET analysis (Table 1) of EG on Li-AHA modification suggests the adsorbed Li-AHA on EG surface, which may also intercalate inside the EG gallery. It is to be noted that the breakdown of 'stacked' EG into smaller crystals or few-layer graphene-like structure in the presence of Li-AHA may be rationalized on the basis that electrostatic charge repulsion between the negative charges of EG and AHA^- (Li-AHA on dissociation leads to Li^+

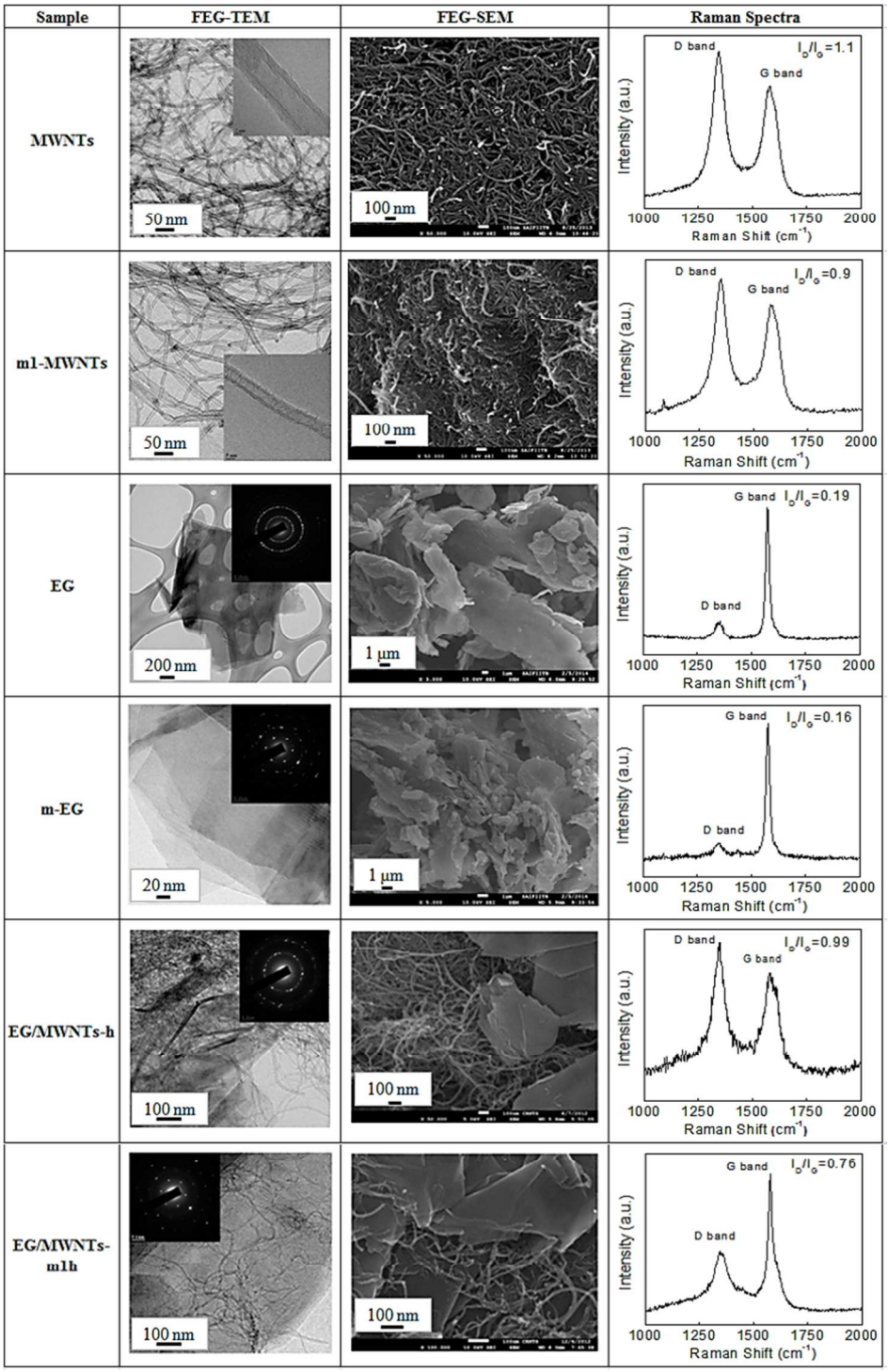

Figure 1: Morphology and the corresponding Raman spectra of MWNTs, EG and EG/MWNTs-h hybrid mixture in the presence of Li-AHA

and AHA^- in the deionized water), wherein AHA^- could enter in the bundles of the EG under ultra-sonication. A similar mechanism postulated in case of debundling of MWNTs in the

presence of Na-AHA may be operative here as well. Further, at higher concentration of Li-AHA, a higher extent of 'de-stacking' of EG layers is observed as Li-AHA do not 're-aggregate' as of classical surfactant due to the structural novelty, wherein, middle segment of Li-AHA serves as hydrophobic, whereas, both the ends exhibit hydrophilic character. This phenomenon could lead to exfoliation of the EG platelets overcoming the van der Walls forces between the layers.

Raman spectrum of pristine EG (Fig. 1) shows the G-band at ~1574 cm^{-1} and the D-band at ~1351 cm^{-1} [28]. Raman spectrum of m-EG exhibits a shift in G-band to 1578 cm^{-1}due to adsorbed Li-AHA on the surface as well as inside the EG gallery. Pristine EG shows I_D/I_G ratio of 0.2, whereas m-EG shows 0.16 due to partial exfoliation of EG in the presence of Li-AHA. The reduction in I_D/I_G ratio for m-EG as compared to pristine EG may be due to increased sp^2 domains due to the exfoliation of EG.

Morphological Investigation of EG/MWNTs hybrid filler is shown in Fig. 1. SEM investigation of unmodified hybrid of EG/MWNTs mixture (EG/MWNTs-h) shows the existence of each filler of individual identity with 'agglomerated' MWNTs and 'stacked' EG. TEM micrograph also shows 'agglomerated' structure associated with MWNTs and 'stacked' EG in the hybrid filler. SAED analysis of EG/MWNTs-h hybrid filler (Fig. 1) shows 'ring-like' pattern due to 'polycrystalline' nature of EG in the hybrid. This observation further substantiates the inability of MWNTs to enter into the gallery of EG under ultra-sonication. SEM investigation (Fig. 1) of EG/MWNTs-m1h hybrid shows m1-MWNTs are 'intercalated' into the partially exfoliated EG gallery, which is also supported by the corresponding TEM observation. SAED analysis of the corresponding EG/MWNTs-m1h hybrid shows a 'hexagonal' dot pattern similar to 'graphene-like' structure of exfoliated EG in the hybrid. This observation confirms the fact that Li-AHA mediates in intercalation of modified MWNTs into the EG gallery under the similar

ultra-sonication condition in DI water. Further, the decrease in specific surface area (Table 1) of EG/MWNTs-h hybrid with Li-AHA modification suggests the adsorption of Li-AHA on the surface of EG/MWNTs-h hybrid. A well-developed 'network-like' structure consisting of GNP/MWNTs and RGO/MWNTs hybrid has been reported earlier [7, 9, 10].

Raman spectrum of EG/MWNTs-h hybrid shows G-band and D-band signature similar to the major component; MWNTs, due to due to their separate identity as shown in Fig. 1. Raman spectrum of EG/MWNTs-m1h hybrid shows the features of both the component EG and m-MWNTs due to improved interaction between the filler. G-band and D band of the hybrid mixture could be de-convoluted to a sharp peak corresponding to EG and a broad peak of m1-MWNTs (not shown here). EG/MWNTs-h hybrid shows I_D/I_G ratio of 0.99, which is close to the major component; MWNTs, whereas EG/MWNTs-m1h hybrid shows I_D/I_G ratio of 0.76 [10] due to the intercalation of m1-MWNTs into the partially exfoliated EG gallery (Fig. 1).

Table 1: Specific surface area of EG, MWNTs and EG/MWNTs hybrid mixture

Sample code	BET surface area (m^2/g)
EG	15
m-EG	5
MWNTs	294
m1-MWNTs	58
m2-MWNTs	6
EG/MWNTs-h	220
EG/MWNTs-m1h	45
EG/MWNTs-m2h	1

b. WAXD analysis of pristine MWNTs, pristine EG and hybrid mixture of EG/MWNTs

Wide angle X-ray diffraction (WAXD) pattern of pristine MWNTs, pristine EG and EG/MWNTs-h hybrid is shown in supplementary Fig. 1. Pristine MWNTs show a diffraction maxima at $2\theta = 25.6°$ corresponding to hexagonal graphitic structure of (002) plane with d-spacing of 0.347 nm [29]. Pristine EG shows an intense crystalline peak at $2\theta = 26.5°$, which is the characteristic of hexagonal graphitic peak of (002) plane with d-spacing of 0.335 nm [29]. EG/MWNTs-h hybrid filler shows diffraction maxima corresponding to both EG and MWNTs, due to the existence of both the phases in the hybrid mixture [10]. The incorporation of Li-AHA in m-MWNTs, m-EG and EG/MWNTs-mh hybrid mixture is evident in the corresponding WAXD pattern as the diffraction pattern shows the signature associated with Li-AHA phase, MWNTs and/or EG.

c. FTIR spectroscopic investigation of PA6 based hybrid nano-composites

FTIR spectra of PA6 composites of EG/MWNTs-m2h hybrid and m2-MWNTs are shown in Fig. 2a and 2b respectively. Peak at 1641 cm^{-1}corresponds to carbonyl (C=O) stretching vibration, which is characteristic of amide I band. Peak at 1543 cm^{-1} assigned to nitrogen–hydrogen (N–H) bending vibration and 1264 cm^{-1} is for carbon–nitrogen (C–N) stretching vibration, which is characteristic of amide II band and amide III band respectively.

FTIR spectra indicate the occurrence of melt-interfacial reaction between amine functional group of Li-AHA and acid end group of PA6 chain [30]. The extent of melt-interfacial reaction can be compared via the relative increase in the amide band (I_{amide}) with respect to a band in the finger print region (I_{1115}, C–C stretching, which is unaffected due to melt interfacial reaction). An increase in the relative intensity of the amide peak (I_{amide}/I_{1115}) with increase in Li–

AHA concentration in various composites suggests higher extent of melt-interfacial reaction during melt mixing as shown in Fig. 2c and 2d.

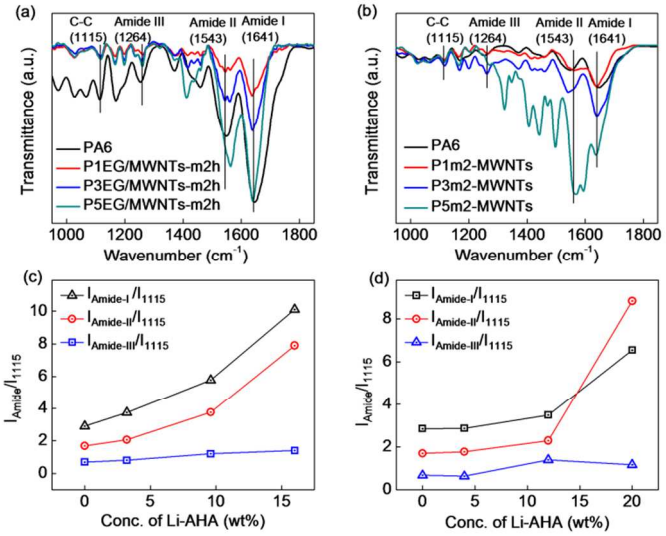

Figure 2: FTIR spectroscopic analysis of PA6 composites of (a) EG/MWNTs-m2h and (b) PA6/m2-MWNTs; Intensity ratio of amide peak to peak at 1115 cm^{-1} of PA6 composite of (c) EG/MWNTs-m2h and (d) m2-MWNTs

A significantly higher extent of melt-interfacial reaction at higher Li-AHA concentration (above 8 wt%) is evident in case of m2-MWNTs and EG/MWNTs-m2h hybrid based PA6 composites (Fig. 2). This may be rationalized on the basis of chain scission phenomenon of the PA6 phase in the presence of Li-AHA. Chain scission and/or plasticization phenomenon of PA6 phase in the presence of Na-AHA has been reported earlier by Bose et al. via the melt-rheological investigation [30]. Further, hybrid composite of PA6 and EG/MWNTs-m2h shows a marginally higher extent of melt-interfacial reaction as compared to PA6/m2-MWNTs composite, which may be due to higher ratio of PA6/Li-AHA (wt/wt) in the respective hybrid composite. Higher chain scission of the PA6 phase may lead to higher extent of melt-interfacial reaction due to the availability of higher fraction of end groups associated with the PA6 chains, which may participate in the melt-interfacial reaction with NH_2 functionality of Li-AHA. A similar observation was earlier reported for PA6/ABS blends with Na-AHA modified MWNTs

[30]. It is also to be noted that Li-AHA engages in interfacial interaction with the PA6 phase and also establishes interaction with both MWNTs and EG. This would perhaps enable PA6 chain to intercalate in the EG gallery and forming a 3-D 'network-like' structure. The influence of modified hybrid in the PA6 matrix to alter the rheological behaviour and electrical conductivity is also noticed [31].

d. Morphology of PA6 based hybrid nano-composites

The dispersion state of MWNTs, EG and EG/MWNTs-h in the PA6 matrix has been investigated via SEM and TEM analysis. Morphological observation of various PA6 based composites at 3 wt% filler concentration via SEM is shown in Fig. 3. 'Agglomerated' MWNTs dispersion along with 'network-like' structure formation is evident in PA6/MWNTs composites (Fig. 3a), whereas finely dispersed MWNTs dispersion is evident in case of the corresponding composite with m1-MWNTs (Fig. 3d). Further, 'stacked' EG platelets is seen in PA6/EG composites (Fig. 3b). A similar morphological investigation of MWNTs and EG based composites has been reported earlier in polycarbonate matrix by Pötschke et. al [21]. Moreover, in case of EG/MWNTs-h hybrid composite (Fig. 3c), 'stacked' EG platelets are seen along with MWNTs. Further, morphological investigation of EG/MWNTs-m1h hybrid composite (Fig. 3e) indicates uniformly dispersed MWNTs along with EG 'platelets' of lesser thickness as compared to unmodified hybrid based composite.

TEM micrographs of PA6/EG/MWNTs-h and PA6/EG/MWNTs-m1h hybrid nano-composites are exhibited in Fig. 4. Morphology (Fig. 4a) of PA6/EG/MWNTs-h unmodified hybrid composite exhibits 'stacked' EG platelets along with MWNTs. SAED pattern corresponding to EG 'platelets' shows a 'ring-like' pattern corresponding to polycrystalline EG.

On the contrary, TEM observation of PA6/EG/MWNTs-m2h modified hybrid nano-composite (Fig. 4b) suggests uniform dispersion of both the filler. Partial exfoliation of EG is observed in the presence of m2-MWNTs as indicated by SAED analysis, which shows the 'hexagonal' dot pattern. This observation suggests the existence of few-layer graphene-like structure in the presence of m2-MWNTs. An interconnecting 'network-like' structure of hybrid filler in the presence of Li-AHA modified MWNTs is also observed in the TEM micrograph (Fig. 4b), which is also supported by the electrical conductivity results [31].

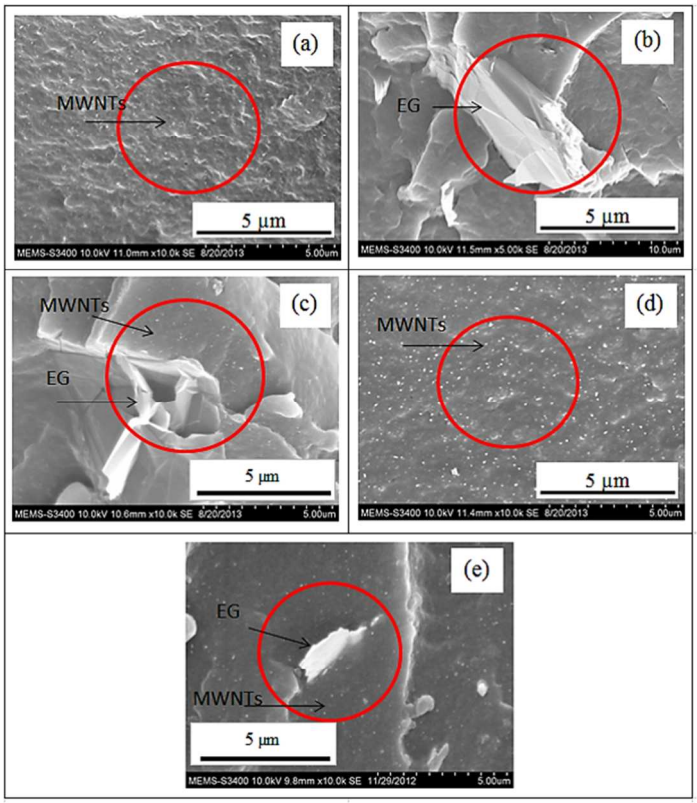

Figure 3: SEM investigation of PA6 composites with 3 wt% (a) MWNTs, (b) EG, (c) EG/MWNTs-h, (d) m1-MWNTs and (e) EG/MWNTs-m1h

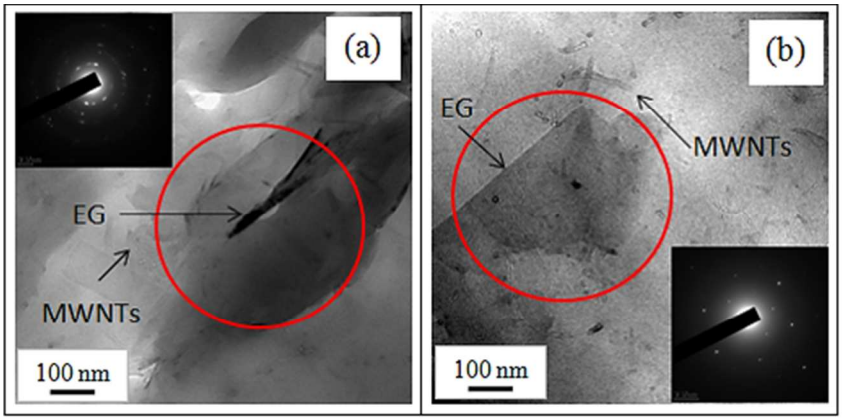

Figure 4: TEM investigation of PA6 composites with 5 wt% of (a) EG/MWNTs-h and (b) EG/MWNTs-m2h hybrid

e. Crystallization behaviour via WAXD of PA6 based hybrid nano-composites

WAXD pattern of PA6 and the corresponding composites of PA6 with EG/MWNTs-h hybrid are shown in Fig. 5 and the corresponding WAXD pattern of PA6/MWNTs and PA6/EG composites are shown in supplementary Fig. 2. PA6 shows the presence of α-crystalline phase and depicts the diffraction maxima at $2\theta = 20.2°$ (α1) and 23.9° (α2), which corresponds to (200) and (002, 202) reflection planes [16]. Addition of carbon based fillers such as MWNTs, EG and EG/MWNTs-h hybrid mixture promote α-crystalline phase of PA6.

It can be seen that the relative intensity of (002) peak of EG increases with increase in EG concentration in PA6/EG composites (supplementary Fig. 2a). Moreover, the full width at half maxima (FWHM) of (002) peak corresponding to EG decreases with increase in EG concentration in the corresponding composite, which suggests a higher extent of 'stacked' EG platelets (See supplementary Table 1). However, MWNTs do not show any signature in the respective PA6/MWNTs composite (supplementary Fig. 2b). Further, (002) peak associated with EG could be observed in the hybrid composites of PA6 (Fig. 5a and 5b). Interestingly, PA6/EG/MWNTs-m1h modified hybrid nano-composites (Fig. 5b) show an increase in FWHM

associated with the (002) reflection of EG (see supplementary Table 1) as compared to PA6/EG/MWNTs-h unmodified hybrid composites as a function of filler concentration, which may be due to the formation of few layer EG in the presence of m1-MWNTs.

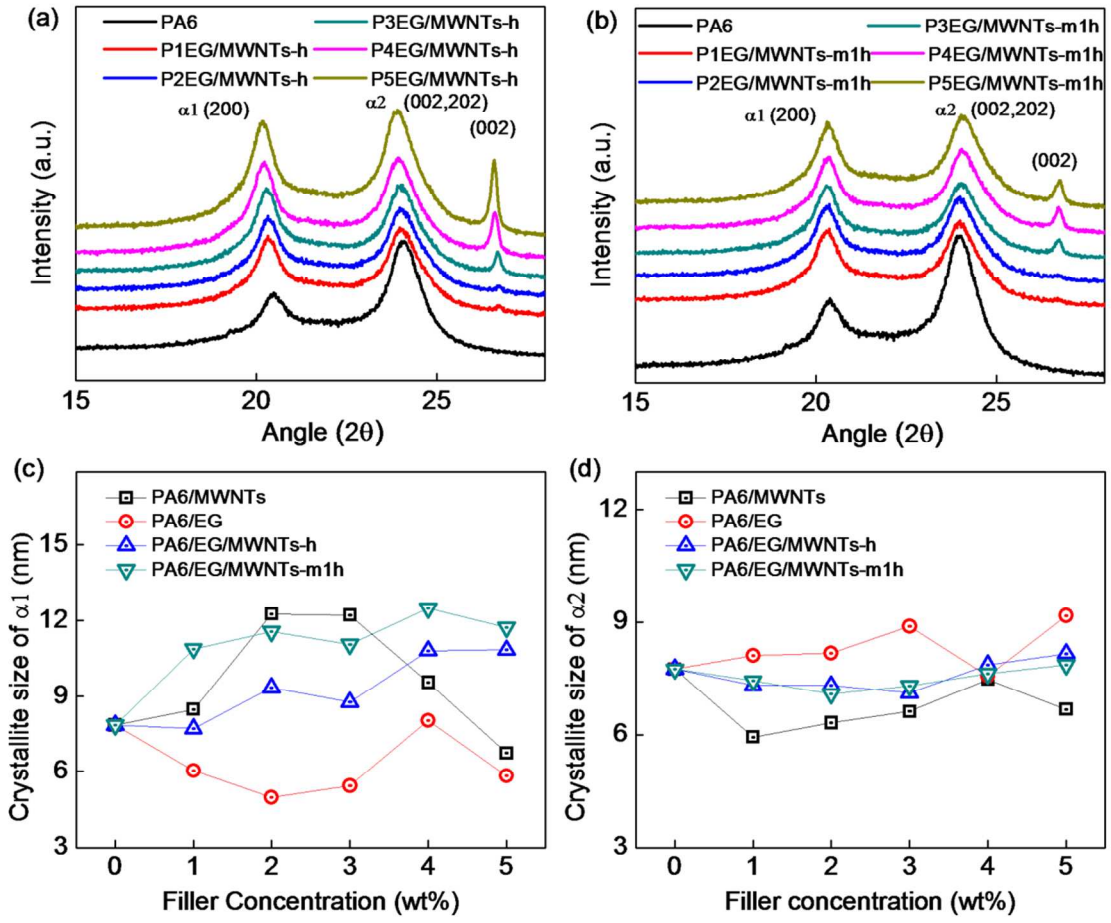

Figure 5: WAXD pattern of PA6 composites of (a) EG/MWNTs-h, (b) EG/MWNTs-m1h; (c and d) Variation in crystallite size of α-crystalline phase of PA6 as a function of filler concentration

The crystallite size corresponding to (200) crystalline plane of PA6 (Fig. 5c) is marginally increased for composites with MWNTs and EG/MWNTs-h unmodified hybrid nano-composites. Further, an increase in the crystallite size of EG/MWNTs-m1h hybrid nano-composite is also observed while using m1-MWNTs in the (200) reflection plane. The crystallite

size corresponding to (002, 202) plane of PA6 in PA6/EG composites do not show any significant variation with increase in EG concentration in the respective composites. In case of PA6/MWNTs composites with MWNTs, EG and EG/MWNTs (Fig. 5c, 5d), crystallite size of PA6 increases as a function of MWNTs concentration corresponding to the (200) plane, whereas, PA6 crystallite size decreases in the direction of (002, 202) reflection plane. Further, EG also favours crystalline orientation of the PA6 phase in the (002, 202) reflection plane as that of pure PA6. This suggests that MWNTs and EG favour the growth of the PA6 crystals in a specific crystalline plane. It is also to be noted that the orientation of the crystalline peak is higher in the direction of (002, 202) reflection plane as compared to (200) crystalline plane in case of pure PA6. However, MWNTs promote the crystalline orientation in both the directions of the reflection planes corresponding to α-crystalline structure, which is also found to be consistent in case of hybrid filler based nano-composites. Moreover, PA6 crystallite size increases as a function of filler concentration in case of modified hybrid based nano-composites in the direction of (200) crystalline plane, which is similar to that of unmodified hybrid based PA6 nano-composites though with a smaller extent.

f. Non-isothermal crystallization and melting behaviour of the PA6 in PA6 based hybrid nano-composites

Melting endotherm of the PA6 phase in PA6/EG/MWNTs-h hybrid composites are shown in Fig. 6a-6b. Neat PA6 shows a melting peak (T_m) at ~219 °C, which corresponds to melting of α-crystalline phase (supplementary Fig. 3). However, the double crystallization peak associated with pure PA6 could be due to 'melting-recrystallization-melting' phenomenon as WAXD analysis suggests only α-crystalline form in pure PA6 as well as in the various composites of PA6.

It is to be noted that PA6/EG, PA6/MWNTs composites and PA6/EG/MWNTs-h hybrid composites do not show any significant variation in T_m in the respective composite with increase in the filler concentration as shown in Fig. 6c. However, in case of composites with m2-MWNTs and EG/MWNTs-m2h hybrid, a marginal reduction in the T_m of the PA6 (Fig. 6c) phase is observed with increase in filler concentration in the respective composite. The reduction in T_m of the PA6 phase in various composites at higher Li-AHA concentration (Fig. 6c) may be due to the miscibility of Li-AHA in the amorphous region of the PA6 phase.

The percentage crystallinity (X_c) of the PA6 phase in PA6/MWNTs, PA6/EG composites and PA6/EG/MWNTs-h hybrid composites is calculated from the melting endotherm and is shown in Fig. 6d. Neat PA6 shows 33% crystallinity, whereas PA6/EG composites show a significant increase in the extent of crystallinity of the PA6 phase with increase in EG concentration in the respective PA6/EG composite. Improvement in the extent of crystallinity may be due to the heterogeneous nucleation provided by EG. The extent of crystallinity of the PA6 phase does not show any significant improvement with increase in MWNTs concentration in PA6/MWNTs composites. EG/MWNTs-h unmodified hybrid based PA6 composites also do not show any considerable improvement in the %crystallinity of the PA6 phase. A significant improvement in %crystallinity of the PA6 phase (44%) is observed with the addition of m2-MWNTs due to improved heterogeneous nucleation provided by modified MWNTs and also due to the higher specific surface area available for nucleation of the PA6 chains. Modified hybrid composites with EG/MWNTs-m2h also show a significant improvement in %crystallinity of the PA6 phase. Li-AHA modified MWNTs and EG/MWNTs-h modified hybrid based PA6 nano-composites show significantly improved %crystallinity of the PA6 phase. It is to be noted that PA6 chains may even crystallize while intercalating inside the EG gallery. Moreover, the

specific surface area related to hetero-nucleating agent in the modified EG/MWNTs hybrid may also increase significantly as compared to unmodified EG/MWNTs hybrid. This may contribute to a higher extent of crystallinity of the PA6 phase in the respective composite. It is also to be noted that Li-AHA may presumably desorb for the EG/MWNTs surface during melt-mixing (due to melt-interfacial reaction), which may otherwise increase the specific surface area corresponds to both MWNTs and EG.

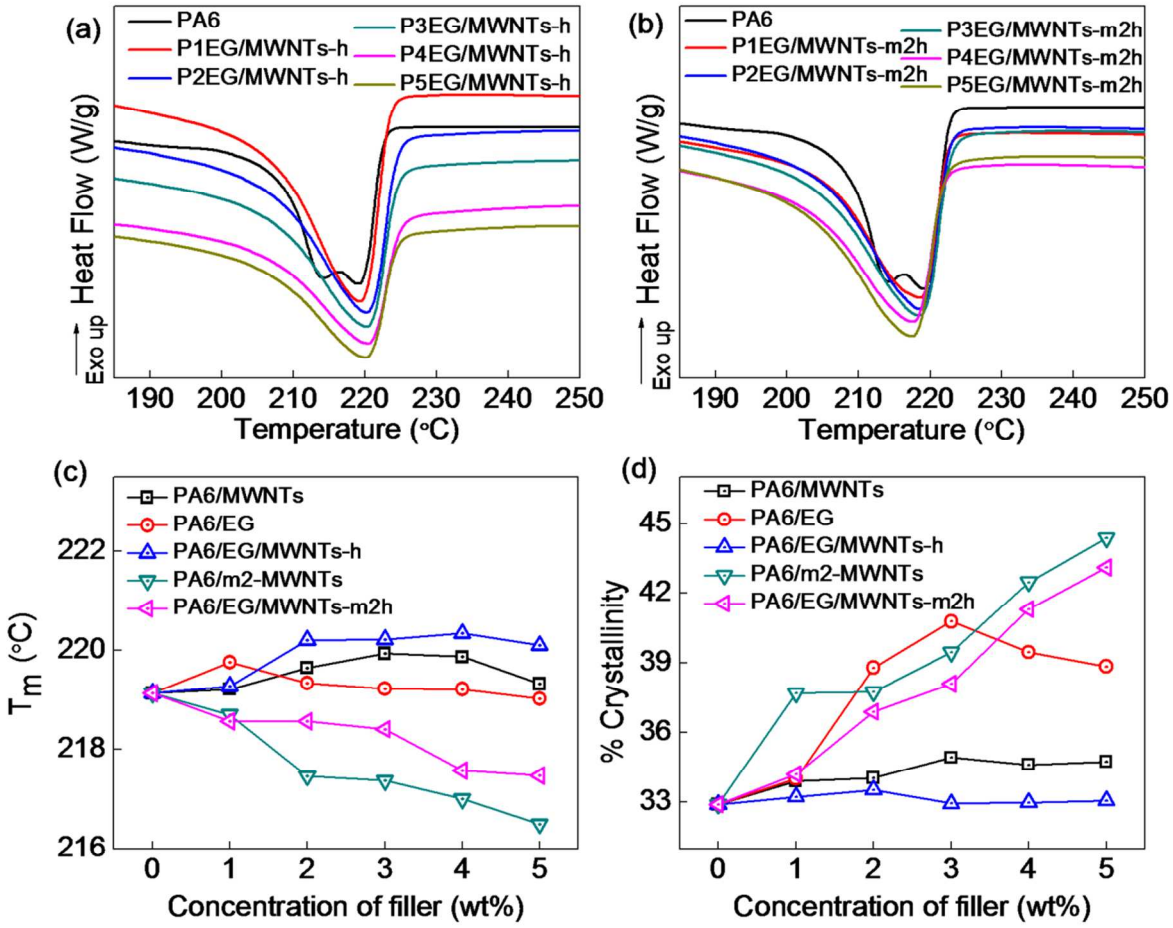

Figure 6: Melting endotherm of PA6 composites of (a) EG/MWNTs-h, (b) EG/MWNTs-m2h; Variation in (c) melting temperature (T_m) and (d) %crystallinity of the PA6 phase in the various composites as a function of filler concentration

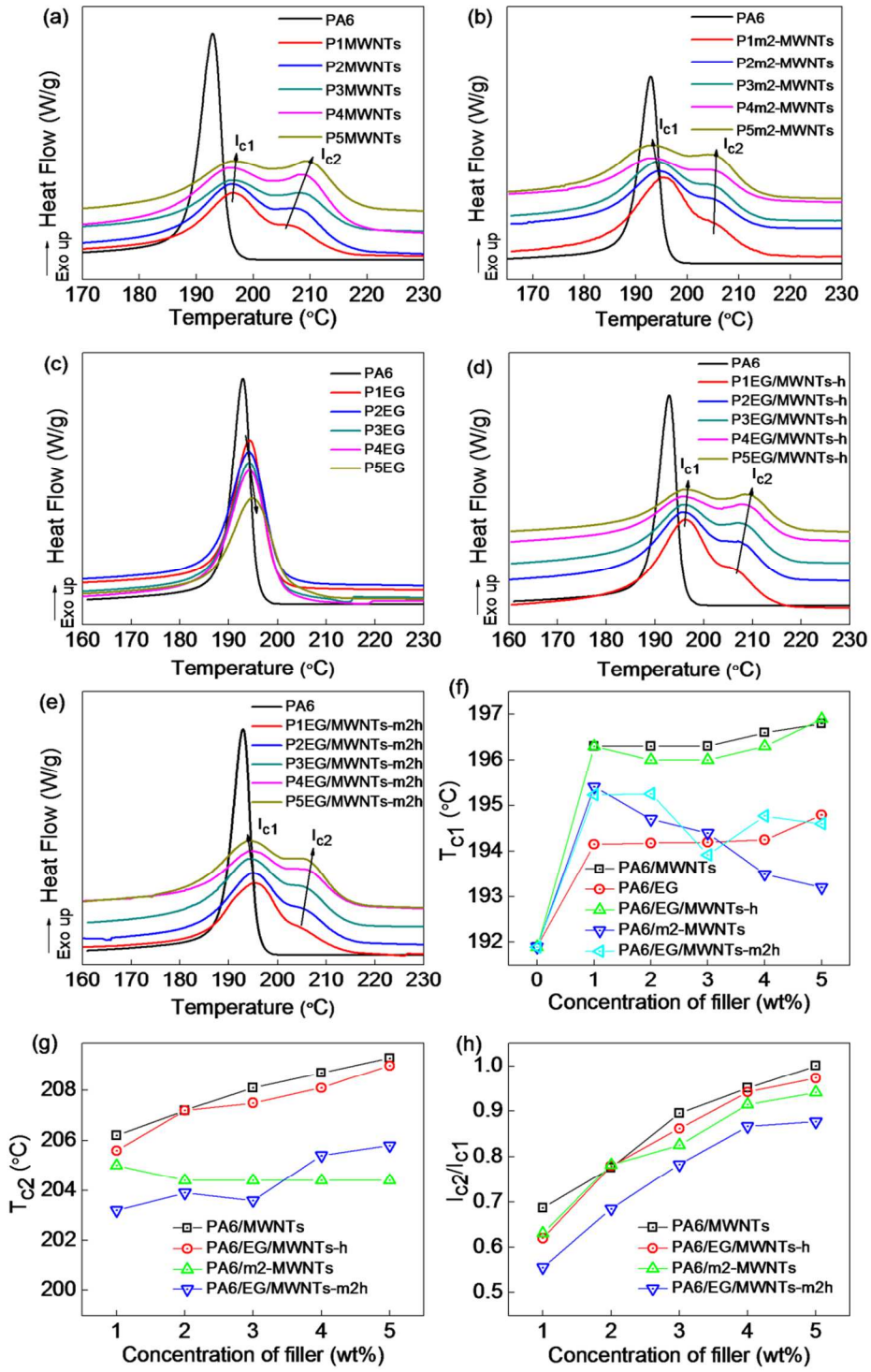

Figure 7: Crystallization exotherm of the PA6 phase in PA6 composites of (a) MWNTs, (b) m2-MWNTs, (c) EG, (d) EG/MWNTs-h, (e) EG/MWNTs-m2h; Variation in (f) T_{c1} and (g) T_{c2} as a function of filler concentration in PA6 based various composites; (h) Ratio of crystallization peaks (I_{c2}/I_{c1}) of MWNTs and EG/MWNTs-h hybrid based PA6 composites

Non-isothermal crystallization behaviour of the PA6 phase in various composites of PA6 is shown in Fig. 7. Neat PA6 shows bulk crystallization temperature (T_{c1}) at ~192 °C. In case of PA6/MWNTs composites, double crystallization exothermic peaks (T_{c1} and T_{c2}) associated with the PA6 phase could be observed (Fig. 7a), which are much higher than the T_{c1} of the PA6 phase, suggesting the heterogeneous nucleating action of the MWNTs. It is also reported that the origin of the second crystallization peak is associated with the 'trans-lamellar crystals' of the PA6 phase due to the crystal lattice matching between PA6 and the MWNTs, wherein PA6 lamella grow perpendicular to the MWNTs surface [11]. A similar observation is also observed (Fig. 7b) in case of PA6/m2-MWNTs composites. On the contrary, PA6/EG composites (Fig. 7c) show a single crystallization temperature (T_{c1}), which shows a shift with increase in EG concentration in the composite indicating hetero-nucleating action of EG. Interestingly, PA6/EG/MWNTs-h and PA6/EG/MWNTs-m2h hybrid composites (Fig. 7d and 7e), show two crystallization peaks corresponding to the PA6 phase, a similar feature which is observed for PA6/MWNTs composites. Moreover, PA6 phase exhibits an increase in T_{c1} with increase in the respective filler concentration (Fig. 7f) suggesting the heterogeneous nucleating action of the filler [11, 15]. An increase in 5-6 °C of T_{c1} of the PA6 phase in various composites is noticed as a function of filler concentration. Further, PA6 composites with m2-MWNTs and EG/MWNTs-m2h (Fig. 7g) also show an increase in T_{c1}, manifesting the hetero-nucleating action of the modified filler. However, T_{c1} shows a decrease at higher filler concentration. The decrease in T_{c1} may be due to Li-AHA mediated chain scission or plasticization effect of PA6 at higher modifier content. In contrast, T_{c2} shows (Fig. 7g) a progressive increase as a function of filler concentration irrespective of the type of the modification of the filler. Moreover, the unmodified EG/MWNTs

hybrid and pristine MWNTs show significantly higher increase in T_{c2} as compared to Li-AHA modified filler.

It is to be noted that the origin of second crystallization peak (T_{c2}) has been explained on the basis of interfacial crystallization of the PA6 phase in the presence of 'individualized' MWNTs, wherein growth of 'trans-crystalline lamellae' of PA6 could take place due to the lattice matching of MWNTs and PA6. Moreover, the origin of T_{c1} could be explained on the basis of heterogeneous nucleation induced by 'agglomerated' MWNTs in the corresponding composite. Hence, the extent of interfacial crystallization [intensity of crystallization peak at higher temperature (I_{c2})/intensity of crystallization peak at lower temperature (I_{c1})] (Fig. 7h) could suggest the extent of MWNTs dispersion as a function of filler concentration in the respective composite. It is seen that the I_{c2}/I_{c1}ratio is increased as a function of filler concentration, which manifests an increased extent of interfacial crystallization [9]. Higher ratio of peak intensity of the crystallization exotherm indicates higher interfacial crystallization, which suggests finer molecular level dispersion of MWNTs along with 'agglomerated' dispersion of MWNTs in the PA6 phase. The value of Ic_1/I_{c2} also suggests a fraction of PA6 chain may also crystallize in the confined layers of EG, wherein PA6 chain may also interact with MWNTs.

Conclusions

Melt-mixed hybrid nanocomposites of EG and MWNTs were prepared with PA6 matrix using a conical twin-screw micro-compounder. A novel organic modifier (Li-AHA) was employed to intercalate Li-AHA modified MWNTs into the partially exfoliated EG gallery. Morphological investigation of EG/MWNTs hybrid filler in the presence of Li-AHA showed an improved interaction between EG and MWNTs. Modified MWNTs could be intercalated into partially exfoliated EG gallery, whereas EG/MWNTs hybrid mixture was observed with separate

identity of MWNTs and EG. Raman spectroscopic analysis of EG/MWNTs hybrid in the presence of Li-AHS showed an up-shift in the G-band due to improved interaction through Li-AHA. The decrease in specific surface area of EG/MWNTs hybrid filler with Li-AHA modification might suggest the adsorption of Li-AHA on the surface of EG/MWNTs hybrid. The melt-interfacial reaction during melt-mixing between acid end group of PA6 and amine functionality of Li-AHA could be indicated through FTIR spectroscopy. The extent of melt-interfacial reaction was increased as a function of Li-AHA concentration in the modified MWNTs and Li-AHA modified EG/MWNTs hybrid. SEM and TEM investigations showed a better dispersion state of EG/MWNTs hybrid filler in the PA6 matrix in the presence of Li-AHA. MWNTs could intercalate in the partially exfoliated EG gallery. WAXD analysis showed the existence of α-crystalline phase of PA6 in various composites of MWNTs, EG and EG/MWNTs hybrid filler. Crystallization studied indicated an increase in bulk crystallization temperature of the PA6 phase in various composites of PA6 due to hetero-nucleating action of the filler. Further, PA6 phase in the presence of MWNTs has exhibited double exothermic crystallization peak due to 'trans-lamellar crystalline' structure of PA6 on MWNTs surface. The formation of 'trans-crystalline lamella' structure of PA6 has increased with increase in MWNTs concentration. A significant increase in the extent of crystallinity of the PA6 phase has been observed in case of EG/MWNTs hybrid filler in the presence of Li-AHA due to improved heterogeneous nucleation provided by the hybrid filler.

In brief, it may be concluded that the crystallization behaviour of the PA6 phase was significantly affected by the Li-AHA modified EG/MWNTs hybrid filler due to improved interfacial interaction between the PA6 phase and the hybrid filler.

Acknowledgements

The authors (ARB and MSS) would like to thank Leibniz Institute of Polymer Research (IPF) Dresden, Germany for providing guest fellowship to carry out part of the research work during their stay (May-July 2013) at IPF Dresden. The authors would like to thank Microcompounder Central Facility, SAIF and CRNTS, IIT Bombay.

References

1. H. Kim, A. A. Abdala, C. W. Macosko, *Macromolecules*, 2010, **42,** 6515-6530.
2. S. B. Sinnott, R. Andrews, *Crit. Rev. Solid State.,* 2001, **26** 145-249.
3. R. Sengupta, M. Bhattacharya, S. Bandyopadhyay, A. K. Bhowmick, *Prog. Polym. Sci.*, 2011, **36,** 638-670.
4. R. H. Baughman, A.A. Zakhidov, W.A. de Heer, *Science*, 2002, **297,** 787-792.
5. X. Huang, Z. Yin, F. Boey, H. Zang, S*mall*, 2011, **7,** 1876-1902.
6. M. K. Shin, B. Lee, S. H. Kim, S. Gambhir, *Nature,* 2012, **3,** 1-8.
7. A. Yu, P. Ramesh, X. Sun, E. Bekyarova, M.E. Itkis, R. C. Haddon, *Adv. Mater.,* 2008, **20,** 4740-4744.
8. Z. Antar, J.F. Feller, H. Noël, P. Glouannec, K. Elleuch, *Mater. Lett.,* 2012, **67,** 210-214.
9. Q. Cheng, J. Tang, J. Ma, H. Zhang, N. Shinya, L. C. Qin, *Phys. Chem. Chem. Phys.*, 2011, **13**, 17615–17624.
10. B. P. Vinayan, R. Nagar, V. Raman, N. Rajalakshmi, S. Ramaprabhu, *J. Mater. Chem.*, 2012, **22,** 9949-9956.
11. A. C. Brosse, S. T. Girault, P. M. Piccione, L. Leibler, *Polymer*, 2008, **49,** 4680-4686.
12. A. R. Bhattacharyya, P. Pötschke, L. Häußler, D. Fischer, *Macromol. Chem. Phys.,* 2005, **206,** 2084-2095.

13. M. Karevan, S. Eshraghi, R. Gerhardt, S. Das, K. Kalaitzidou, *Carbon*, 2013, **64,** 122-131.

14. J. M. Augustine, S. N. Maiti, A. K. Gupta, *J. Appl. Polym. Sci.,* 2012, **125,** 478-485.

15. S. Bose, A. R. Bhattacharyya, L. Häußler, P. Pötschke, *Polym. Eng. Sci.,* 2009, **49,** 1533-1543.

16. M.I. Kohan, Nylon Plastics, John Wiley & Sons, New York, 1973.

17. T. D. Fornes, D. R. Paul, *Polymer*, 2003, **44**, 3945-3961.

18. B. Krause, P. Pötschke, L. Häußler, *Compos. Sci. Technol.*, 2009, **69**, 1505-1515.

19. P. V. Kodgire, A. R. Bhattacharyya, S. Bose, N. Gupta, A. R. Kulkarni, A. Misra, *Chem. Phys. Lett.* 2006, **432,** 480-485.

20. J. Brandrup, Polymer Handbook, John Wiley, New York, 1999.

21. P. Pötschke, M. Abdel-Goad, S. Pegel, D. Jehnichen, J. E. Mark, D. Zhou, G. Heinrich, *J. Macromol. Sci. A*, 2009, **47,** 12-19.

22. R. A. Khare, A. R. Bhattacharyya, A. S. Panwar, S. Bose, A. R. Kulkarni, *Polym. Eng. Sci.,* 2011, **51,** 1891-1905.

23. A. V. Poyekar, A. R. Bhattacharyya, A. S. Panwar, G. P. Simon, D. S. Sutar, *ACS Appl. Mater. Inter.*, 2014, **6,** 11054-11067.

24. H. M Heise, R. Kuckuk, A. Srivastava, B. P. Asthana,. *J. Raman Spectrosc.*, 2011, **42**, 294-302.

25. D. Baskaran, J. W. Mays, M. S. Bratcher, *Chem. Mater.*, 2005, **17,** 3389-3397.

26. L. Z. Bai, D. L. Zao, T. M. Zhang, W. G. Xie, J. M. Zhang, Z. M. Shen, *Electrochim. Acta*, 2013, **107**, 555-561.

27. Y. Hernadez, V. Nicolasi, M. Lotya, A. C. Ferrari, J. N. Coleman, *Nat. Nanotechnol.*, 2008, **3,** 563-568.

28. A. C. Ferrari, *Solid State Commun.,* 2007, **143,** 47-57.

29. S. Cravanzola, G. Haznedar, D. Scarano, A. Zecchina, F. Cesano, *Carbon,* 2013, **62**, 270-277.

30. S. Bose, A. R. Bhattacharyya, A. R. Kulkarni, P. Pötschke, *Compos. Sci. Technol.*, 2009, **69,** 365-372.

31. M.S. Sreekanth, A. S. Panwar, P. Pötschke, A. R. Bhattacharyya, Electrical conductivity and rheological behaviour of polyamide6 based hybrid nanocomposites (manuscript under review).